J. Fluid Mech. (2009), *vol.* 618, *pp.* 181–208.
doi:10.1017/S0022112008004333 Printed in the United Kingdom

Dense, bounded shear flows of agitated solid spheres in a gas at intermediate Stokes and finite Reynolds numbers

HAITAO XU[1]†, ROLF VERBERG[2], DONALD L. KOCH[2]‡ AND MICHEL Y. LOUGE[1]

[1]Sibley School of Mechanical and Aerospace Engineering, Cornell University, Ithaca, NY 14853, USA

[2]School of Chemical and Biomolecular Engineering, Cornell University, Ithaca, NY 14853, USA

(Received 5 September 2007 and in revised form 9 September 2008)

We consider moderately dense bounded shear flows of agitated homogeneous inelastic frictionless solid spheres colliding in a gas between two parallel bumpy walls at finite particle Reynolds numbers, volume fractions between 0.1 and 0.4, and Stokes numbers large enough for collisions to determine the velocity distribution of the spheres. We adopt a continuum model in which constitutive relations and boundary conditions for the granular phase are derived from kinetic theory, and in which the gas contributes a viscous dissipation term to the fluctuation energy of the grains. We compare its predictions to recent lattice-Boltzmann (LB) simulations. The theory underscores the role played by the walls in the balances of momentum and fluctuation energy. When particle inertia is large, the solid volume fraction is nearly uniform, thus allowing us to treat the rheology using unbounded flow theory with an effective shear rate, while predicting slip velocities at the walls. When particle inertia decreases or fluid inertia increases, the solid volume fraction becomes increasingly heterogeneous. In this case, the theory captures the profiles of volume fraction, mean and fluctuation velocities between the walls. Comparisons with LB simulations allow us to delimit the range of parameters within which the theory is applicable.

1. Introduction

We consider sheared suspensions of solid spheres in a gas, in which the spheres interact through binary collisions and possess significant fluctuation velocities. In such agitated flows, collisions contribute to the transfer of momentum and fluctuation energy (see, e.g. Sinclair & Jackson 1989; Louge, Mastorakos & Jenkins 1991; Dasgupta, Jackson & Sundaresan 1994; Bolio, Yasuna & Sinclair 1995; Sundaram & Collins 1997). The Stokes number $St \equiv \tau_v \Gamma$ measures the relative importance of grain inertia and viscous forces acting on a sphere of viscous relaxation time $\tau_v = m/6\pi a\mu_g$, where m is the mass of the sphere, a is its radius, μ_g is the gas viscosity, and Γ is the applied shear rate. The Reynolds number $Re \equiv \rho_g \Gamma a^2/\mu_g$ compares fluid inertia and

† Present address: Max Planck Institute for Dynamics and Self-Organization, Göttingen 37077, Germany.

‡ Email address for correspondence: dlk15@cornell.edu

viscous forces, where ρ_g is the gas density. In this work, we interpret spatial variations of particle fluctuation energy, volume fraction and velocity that are observed in Lattice-Boltzmann (LB) simulations by solving the averaged equations of motion in situations at moderate Stokes number for which the viscous dissipation of particle fluctuation energy is significant.

At large Stokes number, the gas does not significantly affect the particle motion. In the absence of body forces, particles with high St at a solid volume fraction less than the dilatancy onset experience mainly collisional interactions (Onoda & Liniger 1990), and their inertia dominates the momentum transfer in the granular phase. Such 'rapid granular flows' are modelled by a kinetic theory that exploits an analogy between the grains and molecules of a dense gas, thus defining a 'granular temperature'. The Boltzmann equation is solved approximately for the particle velocity distribution, which is then used to calculate the transport coefficients (e.g. Lun *et al.* 1984; Jenkins & Richman 1985). Comparisons with molecular dynamic simulations (see Louge *et al.* 1990, 1993, 2001; Bizon *et al.* 1999) and physical experiments carried out in microgravity (see Louge *et al.* 2000, 2001; Xu, Louge &Reeves 2003) have demonstrated the success of these theories for nearly elastic, weakly frictional grains engaged in collisional interactions. As particle inertia decreases, hydrodynamic interactions among particles progressively cause their particle velocity distribution to deviate from expressions derived for rapid granular flows and, at some point, the kinetic theory must account for interactions between particles and the gas.

Sangani *et al.* (1996) studied simple shear flows of a gas and agitated solid spheres, in which the viscous dissipation plays a role in the fluctuation energy balance of the solids, but the Reynolds number vanishes. In this case, the hydrodynamic interactions among particles can be calculated by solving the Stokes equations for the flow. These authors determined the particle velocity distribution function using a moments method, and obtained constitutive relations for the stress tensor and the energy flux. Their theory compared well with numerical simulations. For dense flows or at high Stokes numbers, they also derived a cruder theory by taking into account the viscous dissipation but assuming a Maxwellian velocity distribution. This simpler theory agreed with more elaborate calculations over a wide range of Stokes numbers when $St/R_{diss} \geqslant 2$, where R_{diss} is a dimensionless coefficient characterizing the viscous dissipation of particle fluctuation energy. Wylie, Koch & Ladd (2003) considered the effects of moderate fluid inertia on gas–solid flows with large particle inertia in unbounded shear flows.

Verberg & Koch (2006) carried out LB simulations to investigate the increase of viscous dissipation of particle fluctuation energy due to fluid inertia. They recorded detailed profiles of flow parameters in sheared gas–particle flows between two bumpy boundaries. They showed that at high Stokes number and low to moderate Reynolds number, the sheared suspension resembles a simple shear flow with nearly Maxwellian particle velocity distribution in the bulk, but with appreciable slip at the boundaries. In this case, the rheology can be captured by a theory developed for unbounded flows using effective shear rates. For lower Stokes numbers, because the bounded flows exhibit substantial variations of solid volume fraction and granular temperature, the theory must account for the role of boundaries.

In this paper, we consider shear flows of nearly elastic, frictionless solids suspended in a gas between two parallel bumpy walls at moderate Stokes numbers and finite Reynolds numbers. We focus on situations where the particle velocity distribution is dominated by granular collisions and hydrodynamic interactions are simply captured by a volumetric rate of viscous dissipation, thus allowing us to derive the transfer

of momentum and fluctuation energy from a granular kinetic theory. We also derive boundary conditions for the particle phase by considering collisional momentum and energy transfer at the bumpy boundaries. The resulting averaged equations together with boundary conditions predict at high Stokes numbers the nearly simple shear flows simulated by Verberg & Koch (2006) and the slip velocities at the bumpy walls. We also report new LB simulations at moderate Stokes numbers with significant viscous dissipation of fluctuation energy. In these cases, the theory captures the role of solid walls in the gas–particle system. We use it to predict spatial variations of particle fluctuation energy, particle volume fraction, and the velocity profiles of particles and gas. In addition, we also ran new LB simulations with inelastic particles. Inelasticity further reduces granular agitation and produces greater deviations from the Maxwellian velocity distribution. Comparison with the LB simulations allows us to delimit the range of parameters for which the theory applies.

We outline the system of governing equations, apply it to the flows of interest, and derive granular boundary conditions in § 2. We then present solutions for fully developed flows, and compare our results with LB simulations in § 3. Although we consider here only shear flows between solid boundaries, the equations that we have developed can be applied to more general cases, e.g. with large relative velocities between the two phases owing to the presence of a pressure gradient.

2. Governing equations

2.1. *Arbitrary flows*

We consider flows of nearly elastic, frictionless spheres of coefficient of normal restitution e at a high enough Stokes number that the velocity distribution of the grains is set by collisional interactions. For such flows, Jenkins & Richman (1985) derived constitutive relations valid up to the order $1-e$ from the Boltzmann equation using Grad's 13-moment method, which Sela & Goldhirsch (1998) improved by a Chapman–Enskog expansion to Burnett order. Assuming the homogeneous cooling of granular agitation, Garzó & Dufty (1999) extended the constitutive relations to spheres of arbitrary inelasticity. Kumaran (2006) and Goldhirsh, Noskowicz & Bar-Lev (2005) also introduced particle roughness, but only focused on weakly dissipative or dilute systems. For dense granular flows of inelastic spheres between two parallel boundaries, we calculated that the theories of Jenkins & Richman (1985) and Garzó & Dufty (1999) have nearly indistinguishable predictions in the parameter range of our interest, $e \geqslant 0.7$ and $0 < \nu \leqslant 0.5$, where ν is the solid volume fraction. (Such concurrence may not arise in flows with much higher gradients of ν, for which Garzó & Dufty (1999) introduced an additional term in the constitutive expression for the flux of fluctuation energy.) Therefore, for consistency with our derivation of boundary conditions up to the order of $1-e$, we adopt the relations of Jenkins & Richman (1985), which we incorporate into the balance equations for granular mass, momentum and fluctuation energy, with added contributions from the gas to the momentum and energy equations:

$$\frac{\partial \rho}{\partial t} + \nabla \cdot (\rho \boldsymbol{u}_s) = 0, \tag{2.1}$$

$$\rho\left(\frac{\partial \boldsymbol{u}_s}{\partial t} + \boldsymbol{u}_s \cdot \nabla \boldsymbol{u}_s\right) = \nabla \cdot \boldsymbol{T}_s + \rho \boldsymbol{f}_s - \nu \nabla P_g + \beta(\boldsymbol{u}_g - \boldsymbol{u}_s), \tag{2.2}$$

$$\tfrac{3}{2}\rho\left(\frac{\partial T}{\partial t} + \boldsymbol{u}_s \cdot \nabla T\right) = -\nabla \cdot \boldsymbol{q} + \boldsymbol{T}_s : \nabla \boldsymbol{u}_s - \gamma_{inelas} - \gamma_{vis} + \gamma_{rel}, \tag{2.3}$$

where $\rho = \nu\rho_s$ is the bulk density, ρ_s is the material density of the spheres, $\boldsymbol{u}_s$ and $\boldsymbol{u}_g$ are the local mean particle and gas velocities, $\boldsymbol{f}_s$ is the acceleration due to body forces on the solid phase, $\boldsymbol{T}_s$ is the solid phase stress tensor, P_g is the gas phase pressure, and β is the drag coefficient.

We note that the mass and momentum conservation equations (2.1) and (2.2) are similar to those derived by Anderson & Jackson (1967). In particular, the presence of the gas phase pressure term $\nu\nabla P_g$ in the particle phase momentum balance equation gives rise to buoyancy, even when the relative velocity between the gas and the particles vanishes. This term also captures the particle force due to an applied pressure gradient that may be used to induce a relative velocity of the gas and particle phases. In studies of porous media flows, such as Hill, Koch & Ladd (2001*a*,*b*), this effect is commonly incorporated within the drag term since the pressure gradient is proportional to the relative velocity between the two phases.

In (2.3), $T \equiv \langle \boldsymbol{C}\cdot\boldsymbol{C} \rangle/3$ is the granular temperature with fluctuation velocity $\boldsymbol{C} \equiv \boldsymbol{c}_s - \boldsymbol{u}_s$ and instantaneous particle velocity $\boldsymbol{c}_s$; γ_{vis} is the volumetric rate of viscous dissipation; and γ_{rel} is the rate of energy production due to the mean relative motion between the gas and particle phases.

In (2.2), the stress tensor is

$$\boldsymbol{T}_s = \left[-P_s + \left(\lambda - \tfrac{2}{3}\eta\right)\nabla\cdot\boldsymbol{u}_s\right]\boldsymbol{I} + \eta\left[(\nabla\boldsymbol{u}_s) + (\nabla\boldsymbol{u}_s)^T\right], \tag{2.4}$$

where P_s is the granular pressure, $\boldsymbol{I}$ is the identity tensor, λ and η are the bulk and shear viscosities, respectively. In (2.4), the first two terms in brackets have the same form as in ordinary collisional granular fluids.

For flows of smooth, slightly inelastic, identical spheres, Jenkins & Richman (1985) derived constitutive relations for pressure, transport coefficients and energy dissipation rate. To the lowest order in $1 - e$, their results are

$$P_s = 4\rho F G T, \tag{2.5}$$

$$\lambda = \frac{8}{3\sqrt{\pi}}\rho\sigma G T^{1/2}, \tag{2.6}$$

and

$$\eta = \frac{8J}{5\sqrt{\pi}}\rho\sigma G T^{1/2}, \tag{2.7}$$

where $\sigma = 2a$ is the sphere diameter. The flux of particle fluctuation energy is

$$\boldsymbol{q} = -\kappa\nabla T, \tag{2.8}$$

with conductivity

$$\kappa = \frac{4M}{\sqrt{\pi}}\rho\sigma G T^{1/2}, \tag{2.9}$$

For $0 \leqslant 1 - e \ll 1$, the rate of collisional dissipation is

$$\gamma_{inelas} = \frac{24}{\sqrt{\pi}}(1-e)\rho\frac{T^{3/2}}{\sigma}G. \tag{2.10}$$

In (2.5) to (2.10), the expression

$$G(\nu) \equiv \nu g_0(\nu) \tag{2.11}$$

incorporates the Carnahan–Starling expression for the pair distribution function at contact (Carnahan & Starling 1969),

$$g(r=\sigma/2)\approx g_0(\nu)=\frac{(2-\nu)}{2(1-\nu)^3}, \tag{2.12}$$

which is valid for $\nu < 0.49$ (Torquato 1995), and $F(\nu)=1+1/(4G)$, $J(\nu)=1+(\pi/12)[1+5/(8G)]^2$, and $M(\nu)=1+(9\pi/32)[1+5/(12G)]^2$.

The corresponding balance laws for the gas are

$$\frac{\partial(1-\nu)\rho_g}{\partial t}+\nabla\cdot((1-\nu)\rho_g\boldsymbol{u}_g)=0, \tag{2.13}$$

$$(1-\nu)\rho_g\left(\frac{\partial\boldsymbol{u}_g}{\partial t}+\boldsymbol{u}_g\cdot\nabla\boldsymbol{u}_g\right)=\nabla\cdot\boldsymbol{T}_g+(1-\nu)\rho_g\boldsymbol{f}_g -(1-\nu)\nabla P_g-\beta(\boldsymbol{u}_g-\boldsymbol{u}_s), \tag{2.14}$$

where $\boldsymbol{f}_g$ is the acceleration from body forces acting on the gas phase, and $\boldsymbol{T}_g$ is the gas phase stress tensor. Because the solid density is much greater than the gas density, we ignore the added mass effect and the history force. For solid spheres in low-Reynolds number shear flows, the effect of the lift force on particles is proportional to $Re^{1/2}/St$ (Clift, Grace & Weber 1978), and thus it is negligible when the Stokes number is large or when the Reynolds number is small.

To close the set of equations (2.1)–(2.3), (2.13) and (2.14), we now provide relations for β, γ_{vis}, γ_{rel} and the stress tensor $\boldsymbol{T}_g$. Sangani *et al.* (1996) determined the rate of viscous dissipation γ_{vis} in simple shear flows at vanishing Reynolds number and Stokes number large enough to achieve a nearly Maxwellian velocity distribution. They obtained

$$\gamma_{vis}=\frac{54\mu_g T\nu}{\sigma^2}R_{diss}(\nu,\varepsilon_m), \tag{2.15}$$

where ε_m is a dimensionless parameter characterizing the breakdown of the lubrication force for small gaps between approaching particles. Sundararajakumar & Koch (1996) calculated the exact non-continuum lubrication force when the gap is comparable to the molecular mean free path of the gas λ_g. Sangani *et al.* (1996) obtained an explicit expression for R_{diss} by solving the Stokes equations for random arrays of particles using a multipole method, in which they assumed that the lubrication force at close contact remains constant when the gap is less than $\varepsilon_m\sigma$. By relating the total energy dissipated during a collision with that calculated from the exact theory of Sundararajakumar & Koch (1996), Sangani *et al.* (1996) found

$$\varepsilon_m=9.76\lambda_g/\sigma, \tag{2.16}$$

and interpreted $\varepsilon_m\sigma$ as a length scale characterizing the importance of non-continuum effects on the lubrication force between two smooth particles at close contact.

For real particles, the breakdown of the lubrication force can also result from surface roughness (Smart & Leighton 1989) and gas compressibility (Gopinath, Chen & Koch 1997). None of these mechanisms exists in the LB simulations. Instead, we use a constant $\varepsilon_m=0.01$ to set the cutoff distance between two spheres, below which forces acting on the spheres are constant.

Verberg & Koch (2006) extended the results of Sangani *et al.* (1996) for negligible fluid inertia to Reynolds numbers up to 40. They captured the rate of viscous dissipation with an effective drag coefficient resisting the fluctuating motion of the particles. This coefficient increases linearly with a Reynolds number based on granular

fluctuation velocity $Re_T \equiv \rho_g \sigma T^{1/2}/\mu_g$. Verberg & Koch (2006) fitted the results in the range $0 < Re_T < 40$ and $0.1 \leqslant \nu \leqslant 0.4$ using

$$R_{diss}(\nu, \varepsilon_m, Re_T) = R_{diss,0}(\nu, \varepsilon_m) + \min\{K_s(\nu) Re_T, [K_s(\nu) - K_l(\nu)] Re_{T,0}(\nu) + K_l(\nu) Re_T\}, \quad (2.17)$$

where

$$R_{diss,0}(\nu, \varepsilon_m) = 1 + \frac{3}{\sqrt{2}}\nu^{1/2} + \frac{135}{64}\nu \ln \nu + 11.08\nu(1 - 4.66\nu + 19.03\nu^2 - 25.15\nu^3) + G(\nu)\ln(1/\varepsilon_m), \quad (2.18)$$

$$\left.\begin{aligned} K_s(\nu) &= \nu(3.3237 - 12.253\nu + 32.970\nu^2) \qquad Re_T < Re_{T,0}, \\ K_l(\nu) &= \nu(2.0233 - 6.4742\nu + 19.773\nu^2) \qquad Re_T > Re_{T,0}, \end{aligned}\right\} \quad (2.19)$$

and $Re_{T,0}$ marks the transition from an initially rapid increase of R_{diss} to a subsequent slower increase with Re_T,

$$Re_{T,0}(\nu) = (0.1729 - 0.3416\nu + 0.5973\nu^2)^{-1}. \quad (2.20)$$

In (2.18), the first three terms are an analytical result in the limit of small ν. In the last term, $G(\nu)$ is proportional to the collision frequency, and $\ln(1/\varepsilon_m)$ characterizes the dissipation of particle fluctuation kinetic energy due to the non-continuum lubrication force preceding each collision. The dependence of R_{diss} on Re_T is analogous to the increase of drag with Reynolds number in a fixed bed, as in the Ergun equation (Ergun 1952).

When considering sedimenting suspensions, Koch & Sangani (1999) pointed out that the relative mean velocity between gas and solids and the corresponding drag force induce additional particle agitation. Koch & Sangani based their expression of the sedimentation drag force on the mean particle velocity relative to laboratory coordinates. Instead, we write their results in terms of the mean relative velocity between gas and particles. The drag coefficient in (2.2) is then

$$\beta = 18\mu_g \nu(1 - \nu)^2 R_{drag}(\nu)/\sigma^2, \quad (2.21)$$

and the volumetric rate of energy production rate in (2.3) is

$$\gamma_{rel} = \frac{162\mu_g^2 \nu(1 - \nu)^2}{\rho_s \sigma^3 \sqrt{T}} |\boldsymbol{u}_g - \boldsymbol{u}_s)|^2 S^*(\nu), \quad (2.22)$$

where

$$S^*(\nu) = \frac{\nu[R_{drag}(\nu)]^2}{2\sqrt{\pi} G(\nu)(1 + 3.5\nu^{1/2} + 5.9\nu)}. \quad (2.23)$$

Koch & Sangani (1999) determined $R_{drag}(\nu)$ from numerical simulations. For $0 < \nu < 0.4$, they found

$$R_{drag}(\nu) = \frac{1 + 3(\nu/2)^{1/2} + \frac{135}{64}\nu \ln \nu + 17.14\nu}{1 + 0.681\nu - 8.48\nu^2 + 8.16\nu^3}. \quad (2.24)$$

For $\nu \geqslant 0.4$, they invoked the empirical correlation of Carman (1937)

$$R_{drag} = \frac{10\nu}{(1 - \nu)^3} + 0.7, \quad (2.25)$$

to which they added the constant 0.7 to match (2.24) and (2.25) at $\nu = 0.4$. Note that the drag coefficient of Koch & Sangani (1999) in (2.24) is for small Reynolds number

based on relative velocity. It is the regime of interest here, because in our shear flows, the relative velocity is appreciable only in a small region near the wall where the gas moves with the latter, while the particles slip. We will return to this discussion in greater detail in § 3.4. For other applications with finite Re, we could replace R_{drag} by the expression of Hill *et al.* (2001*a*,*b*) for random arrays of spheres, assuming that the hydrodynamic interactions are the same as in a fixed bed.

For the moderately high Stokes numbers of interest here, the particle-phase stress is at least 10 times larger than the gas-phase stress (Verberg & Koch 2006). Therefore, a reasonable approximation to the particle-phase properties can be obtained by neglecting the gas-phase inertia and stress in (2.14). However, the fluid-phase stress does influence the detailed fluid velocity profile near the walls. The gas-phase stress tensor $\boldsymbol{T}_g$ can be written as the sum of three terms (Batchelor 1970),

$$\boldsymbol{T}_g = \mu_g[(\nabla \boldsymbol{u}_g) + (\nabla \boldsymbol{u}_g)^T] + \boldsymbol{T}^{pf} + T^{Re}, \tag{2.26}$$

where the first term is the viscous stress, the second term is the particle–fluid stress related to the particle stresslet tensor (Batchelor 1970), and the last term is the Reynolds stress due to the fluctuation of gas velocity caused by the presence of agitated particles. As Verberg & Koch (2006) showed, the Reynolds stress is proportional to gas density and hence it is negligible compared to the particle phase stress unless $St/Re = (2/9)(\rho_s/\rho_g)$ is $O(1)$ or less. Because $St/Re \gg 1$ in all cases considered here, we ignore this contribution to $\boldsymbol{T}_g$. Then, the viscous and the particle–fluid stresses may be modelled using an effective viscosity (e.g. Zarraga, Hill & Leighton Jr 2000). We adopt the correlation of Happel & Brenner (1965)

$$\boldsymbol{T}_g = R_\mu(\nu)\mu_g[(\nabla \boldsymbol{u}_g) + (\nabla \boldsymbol{u}_g)^T], \tag{2.27}$$

where $R_\mu(\nu) = \exp(4.58\nu)$ is the ratio between the suspension viscosity and the viscosity of pure gas. We note that this expression is for suspensions with vanishing Stokes and Reynolds number. To our knowledge, however, there is no expression for fluid phase stress at finite Stokes and finite Reynolds number. Verberg & Koch (2006) observed that the sum of the viscous and particle–fluid stress at intermediate Stokes number is smaller than at vanishing Stokes numbers. However, the only aspect of the predictions presented in the following section that is sensitive to the modelling of the gas-phase stress is the gas velocity profile near the wall. Our LB simulations indicate that the assumption of a nearly Maxwellian particle velocity distribution that underlies the modelling of the particle-phase conservation equations breaks down at a higher Stokes number than that required to allow the gas-phase stress to impact the bulk properties of the suspension.

2.2. *Shear flows between parallel boundaries*

We apply the model outlined earlier to fully developed shear flows between two parallel bumpy boundaries without body forces. The domain is periodic in the flow and vorticity directions, respectively x and z, so that variables change only along the gradient y-direction perpendicular to the boundaries. In this case, the mass of both phases is automatically conserved, the momentum balances in the z-direction vanish and the y-direction momentum balance requires that P_s be constant and P_g be independent of y and z. The only remaining equations are x-momentum balances and the particle fluctuation energy balance.

We write the resulting governing equations in dimensionless form using $y^* \equiv y/Y$, $u_s^* \equiv u_s/U$, $u_g^* \equiv u_g/U$ and $T^* \equiv T/U^2$, where Y is the distance shown in figure 1, U is the relative velocity between the top and bottom boundaries, and u_s and u_g are

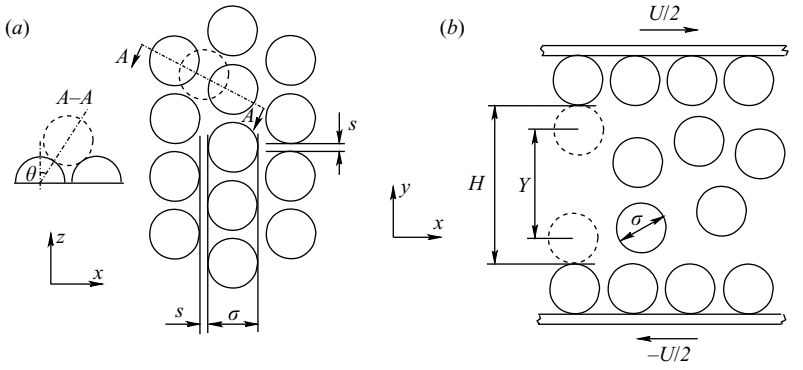

FIGURE 1. Boundaries used in the LB simulations. (*a*) Top view showing spherical wall bumps arranged as a periodic array in the x- and z-directions. Bumps have the same diameter σ as flow spheres. The gap separating them is $s = 0.0274\sigma$. Section A–A illustrates the definition of the penetration angle θ for a sphere in the position shown. (*b*) Side view showing the two parallel boundaries.

the local mean particle and gas velocities in the x-direction. For convenience, we also define the particle fluctuation velocity as $w^* \equiv \sqrt{T^*}$. We make the particle phase pressure dimensionless as $P_s^* \equiv P_s/\rho_s U^2$.

The dimensionless particle phase momentum balance in the flow direction is then

$$\frac{\mathrm{d}^2 u_s^*}{\mathrm{d}y^{*2}} + \left(\frac{1}{P_s^*}\frac{\mathrm{d}P_s^*}{\mathrm{d}y^*} + \frac{1}{J}\frac{\mathrm{d}J}{\mathrm{d}y^*} - \frac{1}{F}\frac{\mathrm{d}F}{\mathrm{d}y^*} - \frac{1}{w^*}\frac{\mathrm{d}w^*}{\mathrm{d}y^*}\right)\frac{\mathrm{d}u_s^*}{\mathrm{d}y^*} + \frac{5\sqrt{\pi}}{8}\frac{1}{JGw^*}\left[(1-\nu)^2\frac{(Y/\sigma)R_{drag}}{St'}(u_g^* - u_s^*) + R_\tau\right] = 0, \quad (2.28)$$

where

$$R_\tau \equiv (-\mathrm{d}P_g/\mathrm{d}x)/\rho_s\sigma(U/Y)^2 \quad (2.29)$$

is the dimensionless gas phase pressure gradient. The mean Stokes number St' is based on U and Y,

$$St' = \frac{m}{3\pi\sigma\mu_g}\frac{U}{Y} = \frac{\rho_s U\sigma^2}{18\mu_g Y}, \quad (2.30)$$

where the prime distinguishes it from another Stokes number based on $H = Y + \sigma$ that we will introduce in § 3. The corresponding dimensionless momentum balance for the gas phase is

$$\frac{\mathrm{d}^2 u_g^*}{\mathrm{d}y^{*2}} + \frac{1}{R_\mu}\frac{\mathrm{d}R_\mu}{\mathrm{d}y^*}\frac{\mathrm{d}u_g^*}{\mathrm{d}y^*} + \frac{18Y/\sigma}{R_\mu}\left[\nu(1-\nu)^2 R_{drag}\frac{Y}{\sigma}(u_s^* - u_g^*) + R_\tau St'\right] = 0.$$

Finally, the dimensionless particle fluctuation energy balance is

$$\frac{\mathrm{d}^2 w^*}{\mathrm{d}y^{*2}} + \left(\frac{1}{P_s^*}\frac{\mathrm{d}P_s^*}{\mathrm{d}y^*} + \frac{1}{M}\frac{\mathrm{d}M}{\mathrm{d}y^*} - \frac{1}{F}\frac{\mathrm{d}F}{\mathrm{d}y^*}\right)\frac{\mathrm{d}w^*}{\mathrm{d}y^*} + \frac{\sqrt{\pi}}{16}\frac{1}{MG}\left[(1-\nu)^2\frac{S^*(\nu)(u_g^* - u_s^*)^2}{St'^2 w^{*3}} - \frac{6(Y/\sigma)R_{diss}}{St'}\right] + \frac{1}{M}\left[\frac{J}{5}\left(\frac{1}{w^*}\frac{\mathrm{d}u_s^*}{\mathrm{d}y^*}\right)^2 - 3(1-e)\left(\frac{Y}{\sigma}\right)^2\right]w^* = 0. \quad (2.31)$$

2.3. *Boundary conditions*

In collisional granular flows, bumpy boundaries conveniently impart momentum and fluctuation energy to the grains. In the kinetic theory for the particle phase, the corresponding boundary conditions are applied at a plane located a particle radius away from the bump crests (Xu *et al.* 2003). Accordingly, this plane is what we mean by the 'boundary' for the particle phase (figure 1).

Momentum and energy transfer at the boundary to the particle phase may be obtained by considering collisional interaction between each flow sphere and the boundary and then integrating over all possible collisions. Jenkins & Richman (1986) assumed a Maxwellian particle velocity distribution to calculate boundary conditions for plane flows of identical smooth inelastic disks interacting with a bumpy wall and for similar flows of spheres. Richman & Chou (1988) refined this calculation by considering a perturbed Maxwellian velocity distribution near the bumpy boundary, and Richman (1988) derived the corresponding boundary conditions for smooth inelastic spheres. These studies all assumed that the mean relative 'slip' velocity between the particles and the wall is small compared with the particle fluctuation velocity. Xu (2003) considered flows of smooth inelastic spheres with a large slip velocity at walls consisting of cylinders with axis perpendicular to the flow direction.

In this study, boundary bumps are arranged in the nearly hexagonal lattice sketched in figure 1. Jenkins & Richman (1986) derived boundary conditions for a bumpy wall with similar geometry. They considered flows of identical smooth inelastic particles interacting with spheres randomly distributed on the wall. To simplify the calculation, they assumed that on average, flow particles penetrate a fixed distance into wall bumps and that the slip velocity is small compared to the fluctuation velocity at the boundary. In this work, we extend their results to flows with large slip velocity using the method described by Xu (2003). If we consider only the normal component of the lubrication forces during collisions between a flow sphere and a wall sphere, we calculate the ratio of shear to normal stress and the dimensionless flux of fluctuation energy at the boundary (see the Appendix for derivation).

$$\frac{S}{N} = \frac{\sqrt{(2/\pi)}(2/3)[2/(1+\cos\bar{\theta}) - \cos\bar{\theta}][1 - \sqrt{\pi/32}(e_w/(1+e_w))(A/St_T)]}{\left[1 + (1/4)\sin^2\bar{\theta}\left(u_{slip}^2/T_w\right)\right][1 - \sqrt{1/8\pi}(e_w/(1+e_w))(A/St_T)]}\frac{u_{slip}}{\sqrt{T_w}}, \tag{2.32}$$

and

$$\frac{Q}{N\sqrt{T_w}} = \frac{S}{N}\frac{u_{slip}}{\sqrt{T_w}} - \frac{\dfrac{\sqrt{8/\pi}}{1+\cos\bar{\theta}}\left[1 + \left(\dfrac{e_w^2}{(1-e_w^2)}\right)\left(\dfrac{A}{St_T}\right)\left(\sqrt{\dfrac{\pi}{8}} - \dfrac{A}{8St_T}\right)\right](1-e_w)}{\left[1 + \frac{1}{4}\left(\sin^2\bar{\theta}\right)\dfrac{u_{slip}^2}{T_w}\right]\left[1 - \dfrac{1}{\sqrt{8\pi}}\left(\dfrac{e_w}{1+e_w}\right)\left(\dfrac{A}{St_T}\right)\right]}\frac{u_{slip}}{\sqrt{T_w}}, \tag{2.33}$$

where S and N are the shear and normal stresses at the wall, Q is the flux of fluctuation energy from the boundary to the flow, u_{slip} is the slip velocity, T_w is the granular temperature of flow particles at the boundary, $St_T \equiv (\tau_v\sqrt{T_w})/\sigma$ is the Stokes number based on fluctuation velocity at the boundary, A is a constant defined in the Appendix, e_w is the coefficient of normal restitution of flow spheres colliding with the bumps, and $\bar{\theta}$ is the average penetration angle. Figure 1 sketches the penetration angle θ at one of many possible contact positions of a flow sphere and boundary bumps.

We obtain boundary conditions for u_s^* and w^* by extending constitutive relations in the bulk to the boundary. For the bottom wall, we find

$$\frac{\tau_{s,xy}^*}{P_s^*} = \frac{2J}{5\sqrt{\pi}F}\frac{\sigma}{Y}\frac{\partial u_s^*}{\partial y^*}\bigg|_{y^*=0} = \frac{S}{N} \tag{2.34}$$

and

$$\frac{q_y^*}{P_s^*\sqrt{T^*}} = -\frac{2M}{\sqrt{\pi}F}\frac{\sigma}{Y}\frac{\partial w^*}{\partial y^*}\bigg|_{y^*=0} = \frac{Q}{NT_w^{1/2}}, \tag{2.35}$$

where $\tau_{s,xy}^* = \tau_{s,xy}/\rho_s U^2$ is the dimensionless granular shear stress, $q_y^* = q_y/\rho_s U^3$ is the dimensionless flux of particle fluctuation energy, and S/N and $Q/NT_w^{1/2}$ are given by (2.32) and (2.33). (Note that we use the symbol $\tau_{s,xy}$ for the xy component of the solid phase stress tensor $\boldsymbol{T}_s$ in order to avoid confusion with the granular temperature.) We then derive expressions for $(\partial u_s^*/\partial y^*)_{y^*=0}$ and $(\partial w^*/\partial y^*)_{y^*=0}$ from (2.34) and (2.35), and similar expressions for the top boundary.

Because the gas fills the entire space between boundary bumps on either side, its domain is larger than that of the grains. For simplicity, we treat the gas boundary condition as a vanishing velocity on planes tangential to the crests of wall spheres, and ignore the small gaps in between. In fact, the LB simulations reveal that the average gas velocity in those gaps is almost identical to the wall velocity.

To capture the gas flow in the regions above wall bumps from which sphere centres are excluded (figure 1), we use the approximate theory proposed by Acrivos & Chang (1986) for transport coefficients near the interface between a porous media and a clear fluid, which agrees well with the numerical results of Sangani & Behl (1989). Although the theory of Acrivos & Chang (1986) could not be derived from first principles, it may be regarded as an interpolation between Darcy's law which applies to the interior of the porous media and the Navier–Stokes (N-S) equations which govern the fluid flow outside the porous media (Brinkman 1949; Sangani & Behl 1989). According to this theory, the mean gas velocity in the excluded volume satisfies

$$\mu_g \frac{\mathrm{d}^2 u_g}{\mathrm{d}y^2} = \frac{\phi(y)}{\nu_b}\beta_b[u_g(y) - U_{wall}], \tag{2.36}$$

where $\phi(y)$ is the area fraction of particles on a plane normal to direction y in the excluded volume, and ν_b and β_b are, respectively, solid volume fraction and drag coefficient in the bulk. Because the solid volume fraction is not uniform in general, we equate ν_b to the volume fraction at a distance $\sigma/2$ away from bump crests, where the closest particle centres can reside (figure 1). We then evaluate β_b from ν_b using (2.21). We also calculate particle area fractions in the excluded volume by integrating all possible contributions from particles with centres in the region $\sigma/2$ to σ away from the crests of wall bumps, where the particle volume fractions are known from the energy balance equation (2.31) and the constraint $P_s = \text{const.}$

3. Comparison with simulations

We compare the predictions of our theory with LB simulations of sheared gas–particle flows between two parallel bumpy boundaries, which Verberg & Koch (2006) discuss in detail. Those authors focused on flows of elastic spheres with high particle inertia, for which the solid volume fraction is nearly uniform in the channel. In this work, we also explore cases with greater variations of solid volume fraction, which may be associated with low particle inertia, large fluid inertia, or granular inelasticity.

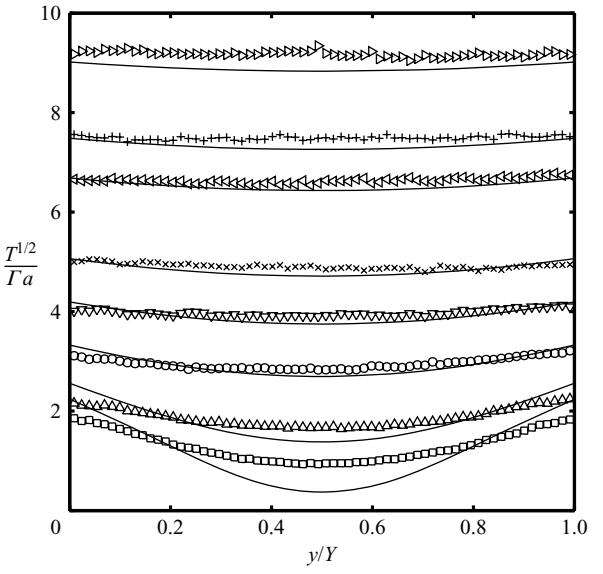

FIGURE 2. Profiles of dimensionless granular fluctuation velocity $T^{1/2}/\Gamma a$ for different St defined in (3.2). Symbols are LB simulations and solid lines are theoretical predictions. Simulation parameters: $H/\sigma = 12$, $Re = 0.1$, $R_\tau = 0$, and $\bar{\nu} = 0.3$. From top to bottom: $St = 100$, 80, 70, 50, 40, 30, 20, 15 and 10.

In our simulations, we impose periodic boundary conditions in the x- and z-directions. We define a Reynolds number based on particle radius and average shear rate $\Gamma = U/H$,

$$Re \equiv \rho_g a^2 \Gamma / \mu_g, \tag{3.1}$$

and a Stokes number slightly smaller than in (2.30),

$$St \equiv \rho_s \sigma^2 \Gamma / 18\mu_g = St' Y/H. \tag{3.2}$$

To isolate the effects of the viscous gas on the flow, we first consider frictionless elastic spheres, $e = e_w = 1$, for which fluctuation energy is dissipated only by viscous forces. We then turn to inelastic particles. Because the kinetic theory has successfully captured their flows for Stokes numbers large enough that the gas plays no significant role (e.g. Xu *et al.* 2003), we now confront our theory with more stringent tests involving inelastic particles at relatively low Stokes number.

3.1. *Stokes number*

Figure 2 shows dimensionless profiles of fluctuation velocity for a range of Stokes numbers and an overall solid volume fraction $\bar{\nu} = 0.3$. Consistent with the predictions of Sangani *et al.* (1996) for simple shear flows, the granular temperature is nearly uniform in the gap in the high-Stokes-number limit, and it decreases with St. However, as the solid agitation declines, the solid boundary plays an increasingly important role in providing fluctuation energy to the flow. As a result, the temperature begins to exhibit a concave profile that betrays a significant transfer of fluctuation energy from the boundary to interior spheres. This effect, which is not present in simple shear flow, is captured well by the present theory.

The observed variations of the granular temperature profiles with Stokes number may be explained by considering the ratio of the granular 'thermal diffusion' time $\tau_{cond} \sim H^2/(\kappa/\nu\rho_s)$ and the dissipation time $\tau_{diss} \sim \tau_v/R_{diss}$. The thermal diffusion time

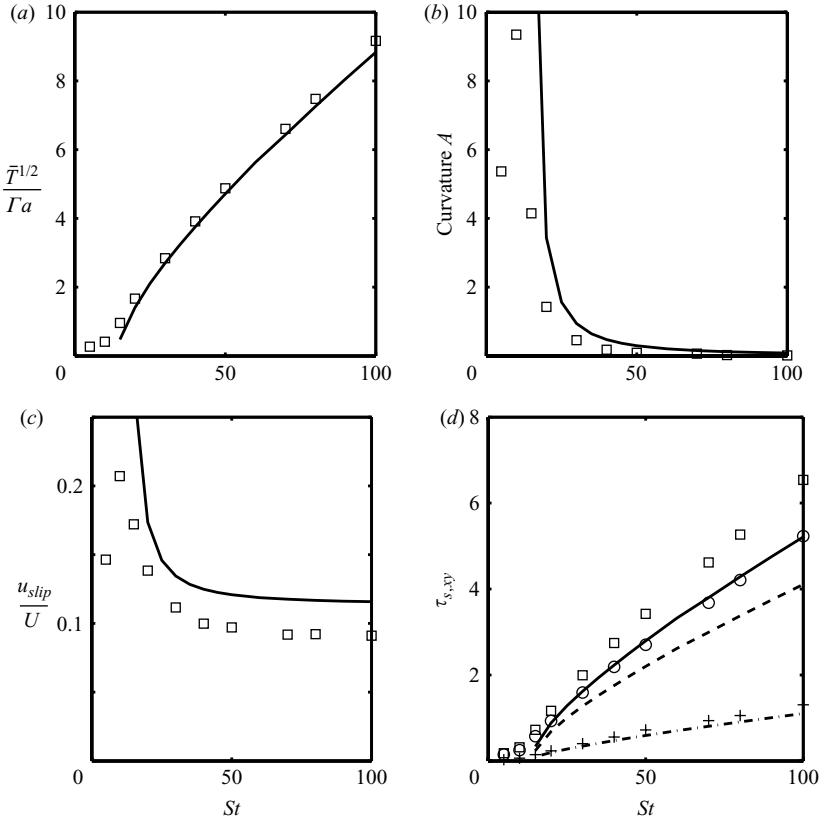

FIGURE 3. Effects of St for $H/\sigma = 12$, $R_\tau = 0$, $Re = 0.1$ and $\bar{\nu} = 0.3$. Symbols are simulations and lines are theoretical predictions. (*a*) Mean dimensionless fluctuation velocity $\bar{T}^{1/2}/(\Gamma a)$; (*b*) curvature A; (*c*) dimensionless slip velocity u_{slip}/U in (3.5); and (*d*) kinetic shear stress $\tau^k_{s,xy}$ (+), collisional shear stress $\tau^c_{s,xy}$ (○), and total shear stress (□), made dimensionless with $\rho_s(\Gamma a)^2$.

measures how long the granular fluctuation energy takes to conduct through the gap between bumpy boundaries; the dissipation time characterizes the viscous dissipation of granular fluctuation energy. When the granular temperature is nearly uniform, we can use the prediction of Sangani *et al.* (1996) for $T^{1/2}/\Gamma a$ in simple shear flow to write

$$\frac{\tau_{cond}}{\tau_{diss}} \propto \left(\frac{H}{\sigma}\right)^2 \left(\frac{R_{diss}}{St}\right)^2. \tag{3.3}$$

Thus, as St decreases, (3.3) shows that the granular temperature generated at the boundary takes a longer time to conduct into the interior and, consequently, it becomes non-uniform.

However, as the Stokes number decreases further, the theory predicts higher granular temperatures, and thus larger temperature gradients at the solid walls, than the simulation. A possible reason for the discrepancy is that the lubrication forces arising from the tangential relative velocity of flow spheres and wall bump are ignored in the current boundary conditions for the particle phase. These tangential forces tend to reduce the slip velocity at the boundary, which in turn results in a smaller production of particle fluctuation energy at the walls. Because of larger

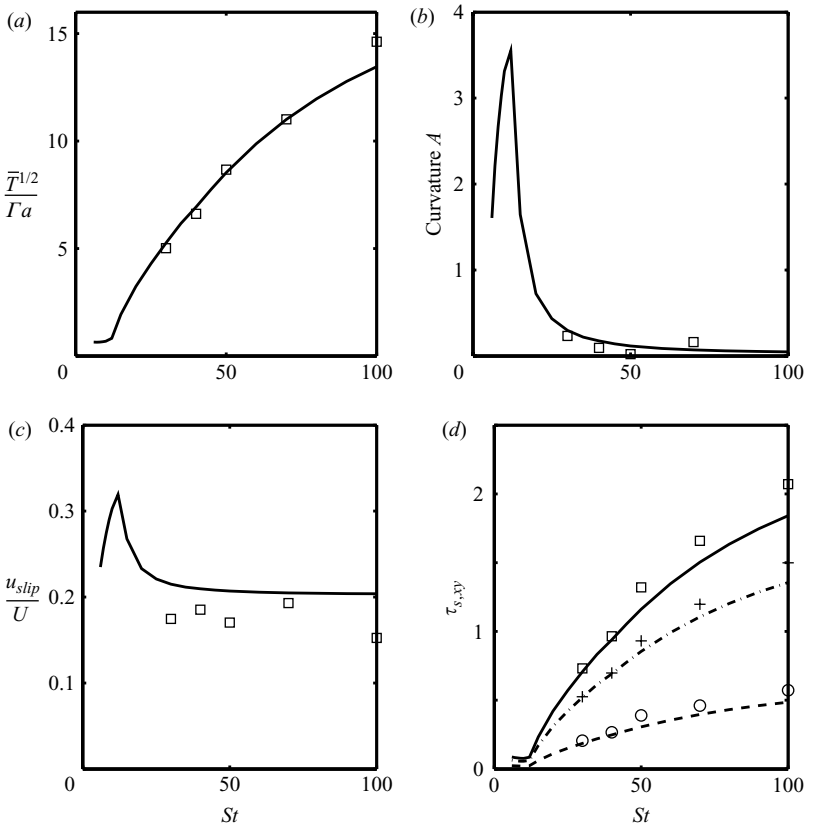

FIGURE 4. As figure 3, but for $\bar{\nu} = 0.1$.

temperature gradients, the predicted temperature profiles are generally more concave than observed in the simulations. Nevertheless, as figure 2 shows, the theory captures temperature profiles well for $St \gtrsim 15$. Here, $St = 15$ corresponds to $St/R_{diss} \approx 2$, below which (2.4) ceases to be valid (Sangani *et al.* 1996). This clearly limits the validity of our assumptions. In particular, when St is too small, it is no longer appropriate to ignore the role of the gas in setting the velocity distribution of the solids.

As figure 2 shows, the fluctuation velocity profile is nearly parabolic for $St \gtrsim 15$. In fact, for dense dry collisional granular flows, Jenkins (2001) showed that the profile of $T^{1/2}$ is a hyperbolic cosine, which is approximately parabolic to the first order. Thus, in order to present results for a wide range of St and $\bar{\nu}$, we fit both the simulation data and the solution of (2.31) to a parabolic function

$$T^{1/2}(y^*) = T_0^{1/2}[1 + A(y^* - 1/2)^2], \tag{3.4}$$

where $T_0^{1/2}$ is the fluctuation velocity at the centre of the channel and A is a measure of the profile's curvature.

Figure 3 shows variations of the average fluctuation velocity $\bar{T}^{1/2} = T_0^{1/2}(1 + A/12)$ and its curvature A with St. It also displays the particle phase shear stresses (Jenkins & Richman 1985; Sangani *et al.* 1996), decomposed into a kinetic contribution $\tau_{s,xy}^k$ corresponding to the diffusive transport of momentum across surfaces, and a collisional contribution $\tau_{s,xy}^c$ arising from direct contacts between particles. Finally, figure 3 shows the mean relative (slip) velocity between the solids and the walls *vs.*

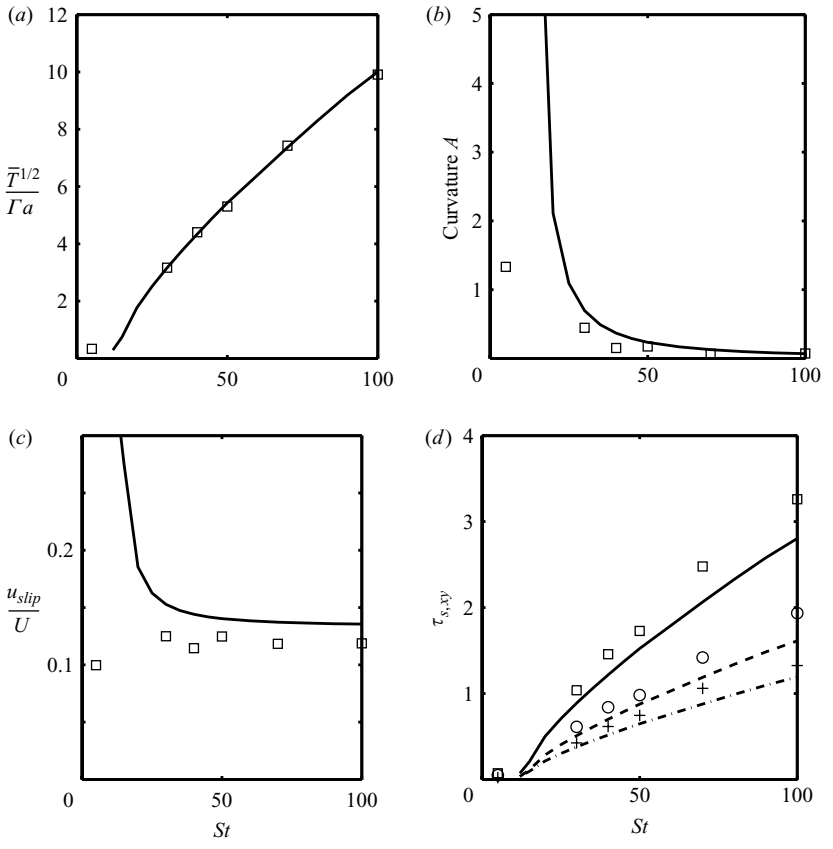

FIGURE 5. As figure 3, but for $\bar{\nu} = 0.2$.

St. Because the channel is symmetric, we plot the average solid slip

$$u_{slip} = |[U_t - u_s(y^* = 1)] + [u_s(y^* = 0) - U_b]|/2, \tag{3.5}$$

where U_t and U_b are the velocities of the top and bottom walls, respectively.

Because the spheres are elastic and frictionless in this case, the viscous dissipation is the only available sink of fluctuation energy (equation (2.15)). Then, the dimensionless granular temperature $T/(\Gamma a)^2$ and, consequently, the granular viscosity, conductivity and stresses grow *ad infinitum* with St. Thus, curvature in the mean velocity and temperature profiles disappears as St increases, and the flow tends to a simple shear flow with constant ν and T, where the temperature is roughly set by a simple algebraic balance between the working of the mean shear $\boldsymbol{T}_s : \nabla \boldsymbol{u}_s$ and the dissipation rate γ_{vis}. The result is a dimensionless fluctuation velocity $T^{1/2}/(\Gamma a)$ that is roughly proportional to St/R_{diss}. As figure 3(a) shows, this behaviour is captured by both theory and simulations.

As $St \to \infty$, the only way to limit the fluctuation velocity in a sheared rapid granular material is to allow collisional energy dissipation. In that case, a similar algebraic fluctuation energy balance would yield an asymptotic $T^{1/2}/(\Gamma a)$ that is a function of ν and impact parameters.

Consistent with Maxwell's observation (Maxwell 1879) of a wall slip proportional to the local granular mean free path $\lambda_s = \sigma/[6\sqrt{2}G(\nu)]$ and the local mean velocity gradient $(\partial u_s/\partial y)_{y=0}$, the relative slip u_{slip}/U scales roughly as $\sigma/[YG(\nu)]$ at moderate

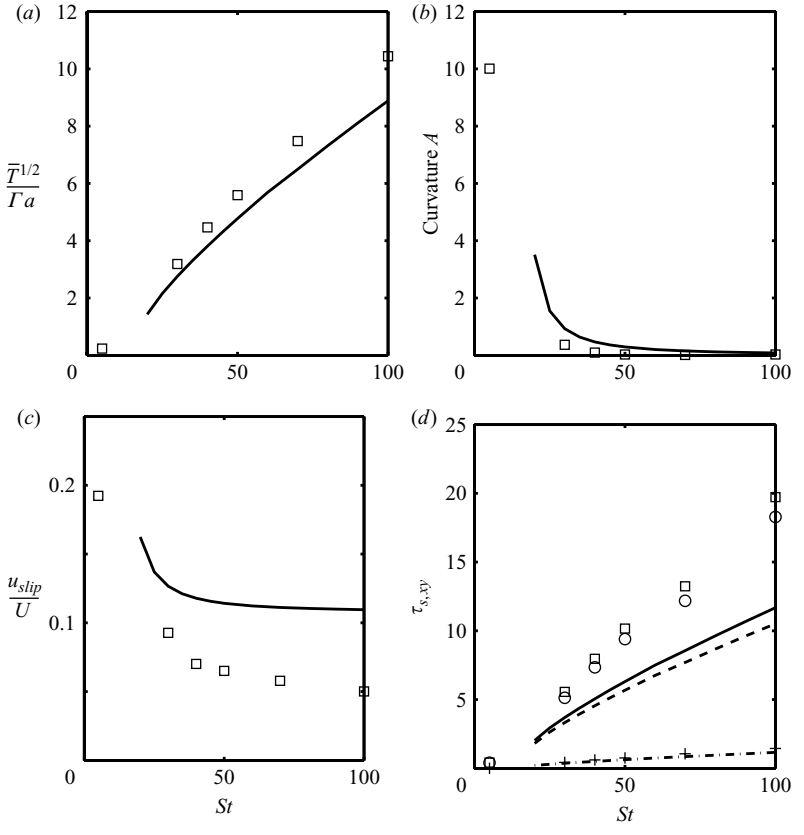

FIGURE 6. As figure 3, but for $\bar{\nu} = 0.4$.

to high St, and thus reaches an asymptote independent of St as $St \to \infty$, once again in agreement with theory and simulations (figure 3*c*).

The role of the bumpy boundary in providing energy to the flow is related to variations of the slip velocity. On the one hand, the particle fluctuation energy generated at the wall is the product of the slip velocity, the shear stress at the boundary, and the surface area of the latter. On the other hand, the energy generated in the bulk is the volume integral of shear stress $\times$ shear rate, which, for almost constant shear rate, is nearly the product of shear stress, mean shear rate and channel volume. Because shear stress is invariant across the channel, the ratio of the particle fluctuation energies produced at the boundary and in the bulk is then approximately the dimensionless slip velocity u_{slip}/U. As St decreases, u_{slip}/U increases, so that more fluctuation energy is generated at the boundary by the working of the shear stress through the mean slip between the grains and the boundary.

Conversely, as St decreases, the temperature profile becomes more curved and the flow no longer resembles a simple shear flow. The wall supplies fluctuation energy to the flow by the working of the shear stress through the granular slip velocity (Jenkins & Richman 1986). In this case, the temperature in the interior is smaller than the temperature at the wall. Then, because the normal stress is constant in this fully developed steady flow, the volume fraction is lowest at the wall. Consequently, $u_{slip}/U \sim \sigma/(YG)$ grows as St decreases. This behaviour of the slip velocity, which is

evident in figure 3(*c*), persists until relatively low values of St. However, as $St \to 0$, particles should again follow the fluid more closely.

3.2. *Solid volume fraction*

As figures 3–6 show, theoretical predictions agree well with LB simulations at overall solid volume fractions $\bar{\nu} = 0.1$, 0.2, 0.3 and 0.4. They both exhibit qualitatively similar behaviour for particle fluctuation velocity, curvature of the temperature profile, mean solid slip and solid stresses.

Because lateral variations of the temperature and volume fraction profiles are less pronounced at lower volume fractions, changes in u_{slip}/U with St become less prominent as $\bar{\nu}$ decreases. However, because the mean free path is longer at smaller ν, the magnitude of the relative slip velocity increases with decreasing volume fraction (figures 3*c*–6*c*).

Solid stresses follow familiar trends in rapid granular flows. At low volume fractions, kinetic stresses are most important. However, because the collision frequency increases rapidly with ν, collisional stresses dominate kinetic stresses for $\bar{\nu} \geqslant 0.3$ (figures 3*d*–6*d*).

As figure 6 shows, theory and simulations differ in fluctuation velocity and shear stresses at $\bar{\nu} = 0.4$. We attribute the discrepancies to anisotropies in the pair distribution function near the wall. Specifically, the theory adopts the isotropic expression of Carnahan & Starling (1969) in (2.12). However, we expect that the wall induces a layering of grains in its vicinity, which becomes more crucial to the stresses as ν grows. Similarly, because R_{diss} was obtained for isotropic configurations of spheres, it may not always capture the viscous dissipation in the presence of particle layering. To test the conjecture that layering at the wall plays a role, we used the algorithm of Hopkins & Louge (1991) to simulate flows of nearly elastic spheres with restitution progressively approaching unity ($0.9 \leqslant e = e_w \leqslant 0.9999$) in the same geometry as the LB simulations, but without gas. For $\bar{\nu} = 0.4$, we observed the same discrepancy in shear stresses between simulations and kinetic theory using the Carnahan–Starling pair distribution, whereas the two agreed well for $\bar{\nu} = 0.3$. Nonetheless, other mechanisms may be responsible for the discrepancies. In particular, although Sangani *et al.* (1996) reported no deviation from the isotropic pair distribution with ν as large as 0.45 in unbounded simple shear simulations, they also measured higher fluctuation velocities at that volume fraction than the predictions of the simple shear-flow theory.

3.3. *Reynolds number*

Figure 7 shows variations of the dimensionless average fluctuation velocity, the curvature of its lateral profile, the relative slip velocity, and solid shear stresses with the inverse of the Reynolds number for fixed $H/\sigma = 12$, $St = 100$, $R_\tau = 0$ and $\bar{\nu} = 0.3$. Broadly, we find that increasing Re (figure 7) has the same effect as decreasing St (figure 3). This relation is evident in simple shear flows of elastic frictionless spheres. There, because the granular temperature is solely determined by the ratio St/R_{diss} (Sangani *et al.* 1996), and because R_{diss} increases linearly with Re_T (equation (2.17)), an increase of the Reynolds number or a reduction in the Stokes number both contribute to decreasing St/R_{diss}. Curiously, because $\bar{T}^{1/2}/\Gamma a$ increases with decreasing Re, Re_T can remain large even when Re is small. Consequently, results continue to depend on Re down to values as small as $Re \approx 0.1$.

Although our bounded shear flows do not produce a uniform Re_T, flows that share comparable ratios St/R_{diss}, in which R_{diss} is calculated from $\bar{T}^{1/2}$ and $\bar{\nu}$, exhibit similar profiles of temperature, volume fraction and mean particle velocity, despite having widely different St and Re (figure 8).

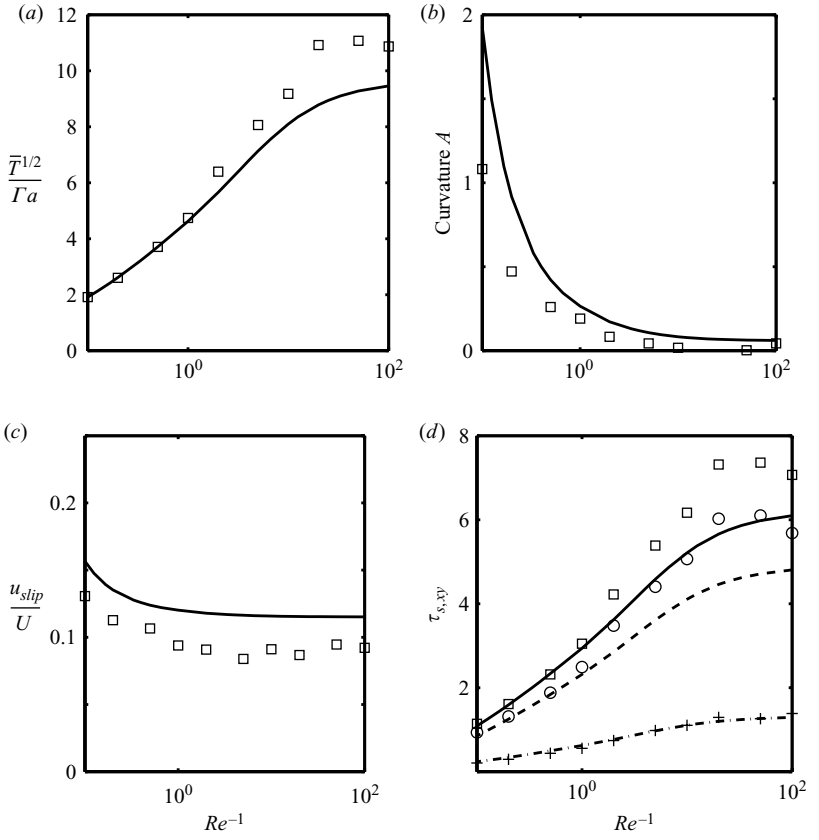

FIGURE 7. Effects of Re defined in (3.1) on theory and LB simulations for $H/\sigma = 12$, $St = 100$, $R_\tau = 0$ and $\bar{\nu} = 0.3$. Graphs and symbols, see figure 3.

3.4. *Channel width*

We investigated the effects of channel width by varying H/σ from 6 to 18, while keeping $St = 20$, $Re = 0.1$ and $\bar{\nu} = 0.3$ constant (figure 9). The granular temperature is nearly uniform in the narrowest channel. In wider channels, the fluctuation velocity rises near the wall and decreases in the interior, and thus the centreline solid volume fraction increases with width.

At first sight, this behaviour may seem counterintuitive. We might expect that, as H/σ increases, the boundaries would play a lesser role in the bulk, therefore creating a simple shear flow there. In fact, because grains in the bulk derive their agitation from the working of shear forces competing with the local volumetric rate of collisional energy dissipation, and because the agitation sets the magnitude of the viscous transport of momentum, the granular temperature in the bulk decays with increasing channel width, thus reducing the velocity gradient there. For large enough H/σ, the agitation collapses and the collisional theory breaks down altogether. Such behaviour is common in dry granular flows, where solid boundaries can only maintain agitation to a limited depth into the flow (e.g. Mueth *et al.* 2000; Jenkins 2001). In experiments that probably involved impulsive as well as longer-range enduring granular interactions, Mueth *et al.* (2000) observed that granular temperature decays exponentially away from a moving boundary. In dense rapid granular flows, Jenkins

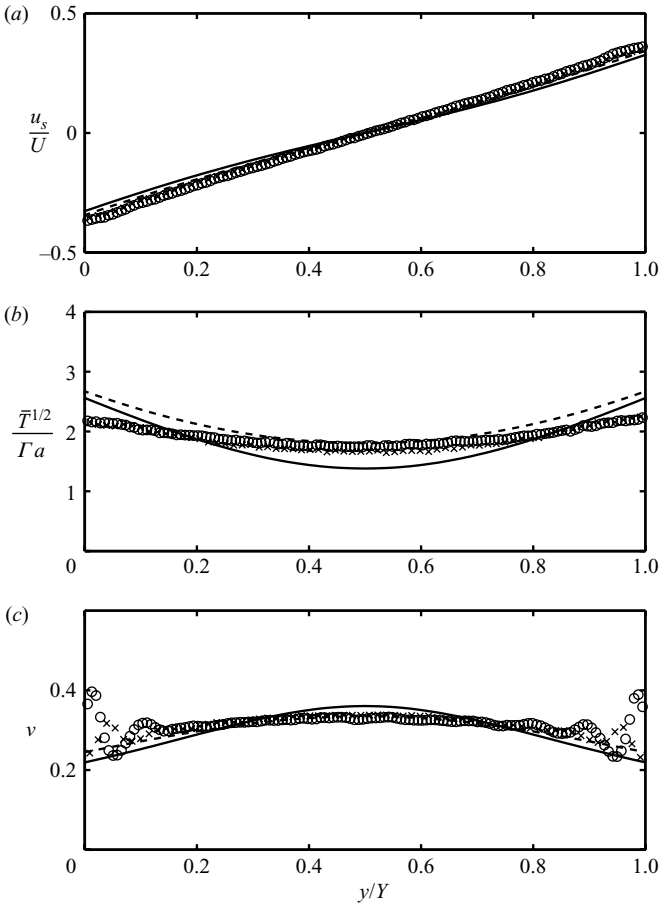

FIGURE 8. Comparison of transverse profiles in flows having roughly the same St/R_{diss}, but widely different St and Re, and $H/\sigma = 12$ and $\bar{\nu} = 0.3$. Symbols are LB simulations and lines are theoretical predictions. Circles and dashed lines: $St = 100$ and $Re = 10$, leading to $St/R_{diss} \simeq 3.2$; crosses and solid lines: $St = 20$, $Re = 0.1$ and $St/R_{diss} \simeq 2.7$. (*a*) Dimensionless mean particle velocity u_s^*; (*b*) dimensionless fluctuation velocity $\bar{T}^{1/2}/(\Gamma a)$; (*c*) solid volume fraction.

(2001) showed that the fluctuation velocity decays as a hyperbolic cosine function of distance from the wall. For gas–solid flows in the dense limit, a simple balance of the flux gradient $\nabla \cdot \boldsymbol{q}$, the shear production $\boldsymbol{T}_s : \nabla \boldsymbol{u}_s$, and the viscous dissipation term γ_{vis} yields a similar result:

$$(T^+)^{1/2}(y^*) = [(T^+)^{1/2}(y^* = 0) - B]\frac{\cosh(k(y^* - 1/2)Y/\sigma)}{\cosh(kY/2\sigma)} + B, \tag{3.6}$$

where $T^+ \equiv T/(\Gamma a)^2$,

$$k \equiv \sqrt{\frac{1}{M}\left[\frac{3\sqrt{\pi}}{2G}\frac{Re}{St}K - \frac{5\pi F^2}{4J}\left(\frac{\tau_{s,xy}}{P_s}\right)^2\right]},$$

$$B \equiv \frac{3\sqrt{\pi}}{4G}\frac{R_{diss,0}}{St}\frac{1}{Mk^2}\frac{H}{Y},$$

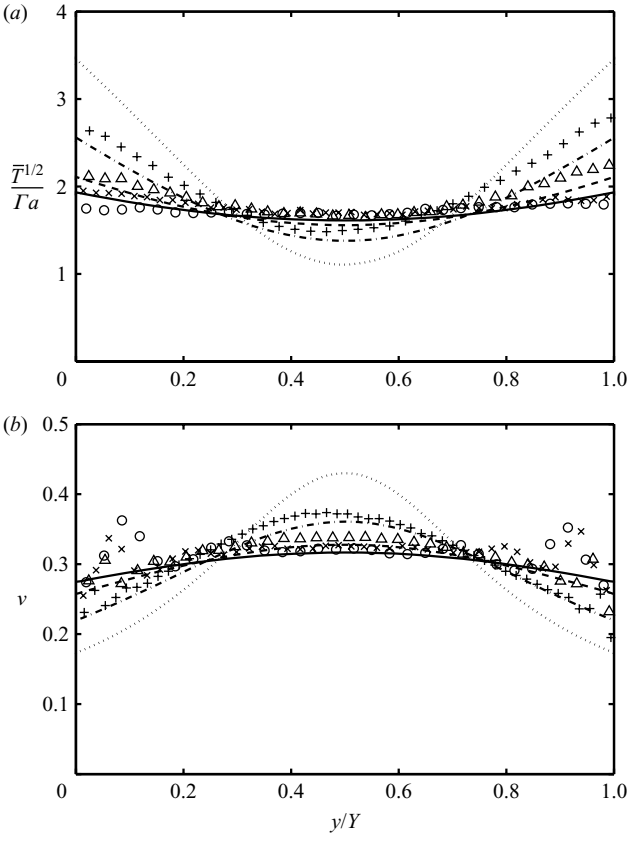

FIGURE 9. Transverse profiles *vs.* dimensionless channel width H/σ for $St = 20$, $Re = 10$ and $\bar{\nu} = 0.3$. (*a*) Dimensionless fluctuation velocity $T^{1/2}/(\Gamma a)$; (*b*) solid volume fraction. Symbols are LB simulations and lines are theoretical predictions; $H/\sigma = 6$ (circles and solid lines), 8 (crosses and dashed lines), 12 (triangles and dash-dotted lines), and 18 (pluses and dotted lines).

and K is either $K_s(\nu)$ or $K_l(\nu)$ defined in (2.19), whichever is appropriate. Equation (3.6) implies that the granular temperature decays faster with y^* as Y/σ increases, a prediction that is consistent with LB simulation data.

Another way to understand the effect of channel width on granular temperature is to consider the ratio of τ_{cond} and τ_{diss} defined in § (3.1). As (3.3) shows, τ_{cond}/τ_{diss} increases with H/σ. Therefore, the flow becomes less uniform as the channel widens. In doing so, it progressively develops a dense, almost static, core region and a dilute agitated sheared band near the walls. This phenomenon is captured by the theory. Because the number of particles in LB simulations and, consequently, the computer time increase with channel size, we did not generate data for very wide channels. However, results for $H/\sigma = 18$ in figure 9 reveal an increase in solid volume fraction at the centreline.

Liss, Conway & Glasser (2002) showed that, for gravity-driven collisional granular flows in a vertical channel, transverse non-uniformities may lead to density waves in the flow direction. In our flow with small St and/or large H/σ, the same instability mechanism could arise. In fact, at large channel width, our continuum theory predicts a highly non-uniform solid volume fraction tending to random close packing near

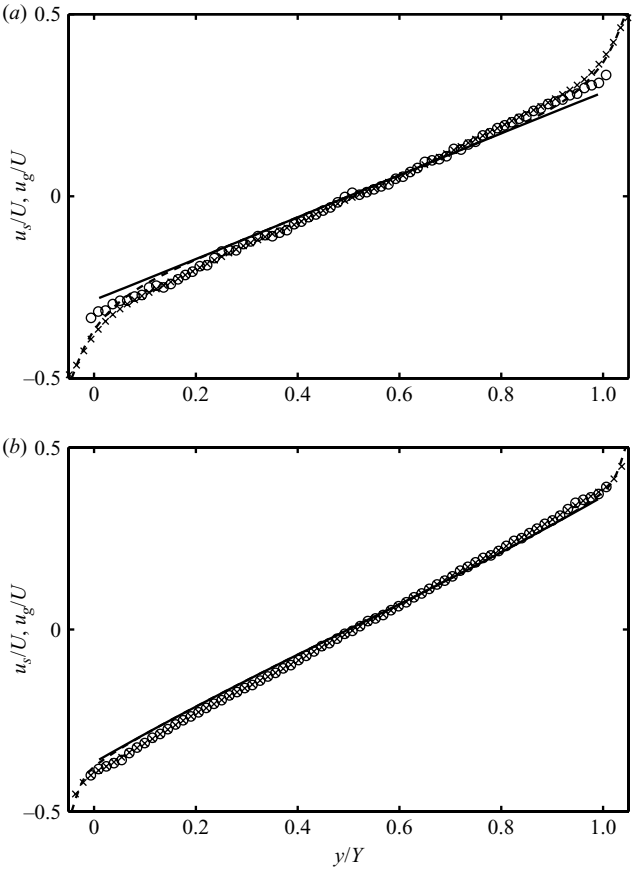

FIGURE 10. Transverse profiles of mean gas and particle velocities for $St = 30$, $Re = 0.1$, $H/\sigma = 12$, (*a*) $\bar{\nu} = 0.1$ and (*b*) $\bar{\nu} = 0.3$. Symbols are LB simulations and lines are theoretical predictions; solid lines and circles: mean solid velocities u_s/U; dashed lines and crosses: mean gas velocities u_g/U.

the centre of the channel, which could betray the onset of instabilities. However, the relatively limited channel lengths of our LB simulations may have prevented the onset of such instability.

Because the average gas velocity is nearly identical to that of the solid phase, we did not mention it in the preceding figures and discussions. To illustrate this, figure 10 compares the dimensionless gas and solid velocities at $\bar{\nu} = 0.1$ and 0.3. The simulations only reveal a noticeable difference between u_g and u_s near the walls under the most dilute conditions, which is captured well by our continuum theory. The theory also predicts well the depth of the region where the relative velocity between the two phases is appreciable. The small relative velocity results in a very small contribution from the gas phase to the production of particle fluctuation energy, i.e. S^* in (2.22). Consequently, the viscous gas acts almost solely as an additional dissipation mechanism for particle fluctuations. Moreover, our treatment of boundary conditions for the gas phase at the solid walls may be justified by the agreement between the theoretical predictions and simulation results of gas velocity in the 'excluded volume' near the solid boundaries.

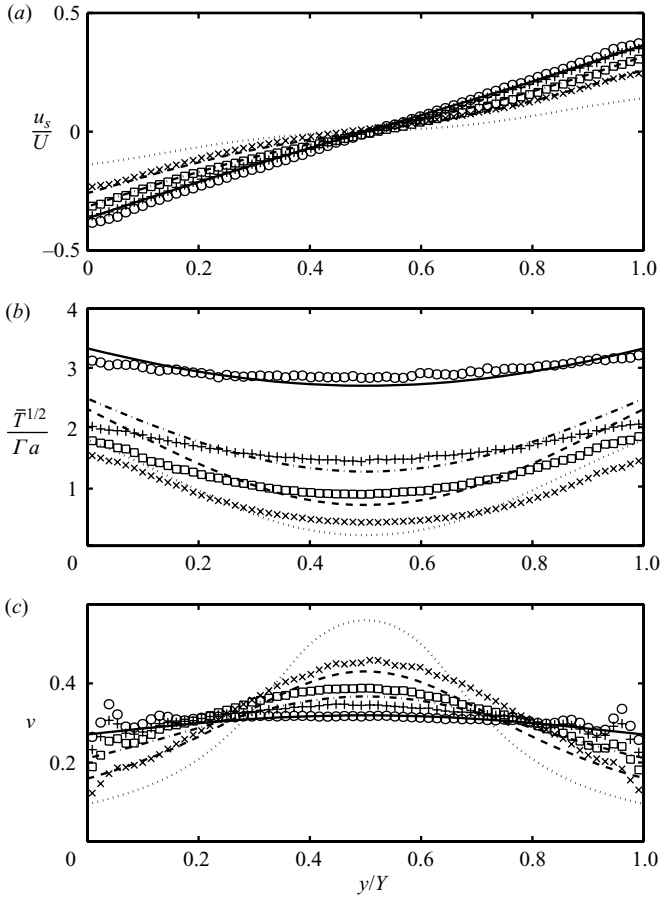

FIGURE 11. Transverse profiles in flows of inelastic spheres, $St = 30$, $Re = 0.1$, $H/\sigma = 12$ and $\bar{\nu} = 0.3$. Symbols are LB simulations and lines are theoretical predictions. Circles and thick solid lines: $e = 1$, pluses and dash-dotted lines: $e = 0.95$, squares and dashed lines: $e = 0.9$, crosses and dotted lines: $e = 0.8$. (*a*) Dimensionless mean particle velocity u_s^*; (*b*) dimensionless fluctuation velocity $\bar{T}^{1/2}/(\Gamma a)$; (*c*) solid volume fraction.

3.5. *Inelasticity*

When particles are inelastic, the additional dissipation of particle fluctuation energy due to inelastic collisions will cause the assumptions in our theory to breakdown at higher Stokes numbers and/or lower Reynolds numbers. In fact, it is known that even for pure granular flows, the constitutive relations derived from kinetic theory become inaccurate as inelasticity increases (Bizon *et al.* 1999). Numerical simulations of inelastic granular flows indicate that the mean flow profiles predicted by kinetic theory agree with simulations as long as $e \gtrsim 0.7$. In figure 11, we compare the predictions of our theory for gas–solid flows with LB simulations for spheres with coefficient of restitution $e = 1$, 0.95, 0.9 and 0.8, respectively. Other parameters are $St = 30$, $Re = 0.1$ and $\nu = 0.3$. In the case of homogeneous flows, the viscous dissipation can be incorporated into an effective coefficient of restitution as

$$e_{eff} = e - \frac{15\pi R_{diss}^2}{128 J G^2 St^2}\left[1 + \sqrt{1 + \frac{256 J G^2 St^2}{R_{diss}^2}(1-e)}\right]. \tag{3.7}$$

For the conditions of figure 11 and with a constant $\bar{\nu} = 0.3$, (3.7) yields $e_{eff} = 0.96$, 0.88, 0.82 and 0.69 for $e = 1$, 0.95, 0.9 and 0.8, respectively. However, we do not expect (3.7) to hold across the entire channel at the lowest elasticity. In this case, higher volume fractions at the centre of the channel enhance viscous dissipation. This produces local values of e_{eff} that are lower than their global estimate based on $\bar{\nu}$, thus probably causing greater deviations from theoretical predictions. Nonetheless, as in pure granular flows, profiles predicted by the theory agree well with simulations for $e_{eff} \gtrsim 0.7$.

4. Conclusions

In this paper, we considered flows of a gas and agitated solids sheared between two parallel bumpy walls at moderate Stokes numbers and small to moderate particle Reynolds numbers. We developed and solved a set of averaged equations in which the particulate phase is treated using a granular kinetic theory and the gas gives rise to interphase drag forces, a viscous stress, and, most importantly, a viscous dissipation of the granular kinetic energy.

In general, bounded shear flows differ from unbounded simple shear by developing substantial particle slip velocity at the wall and profiles of flow variables across the channel. At large Stokes numbers, the flow is nearly uniform and, as Verberg & Koch (2006) observed, the rheology can be modelled using an unbounded flow theory with an effective shear rate. Our theoretical predictions agree well with simulations and can be used to calculate the effective shear rate required in such simple unbounded flow theory.

At intermediate Stokes numbers, bounded flows are no longer homogeneous. Energy is produced at the walls and is transported inward by granular conduction. However, the dissipation of energy due to viscous effects and particle inelasticity substantially reduces the granular temperature in the middle of the channel at smaller Stokes numbers and/or smaller coefficients of restitution. Our predicted profiles of the particle volume fraction and the mean and fluctuation velocity compare well with the LB simulation results for $e = 1$ and overall Stokes numbers as low as ~ 15 and for $St = 30$ and $e \geqslant 0.9$. The theory captures the effects of Reynolds number, channel width, particle volume fraction and inelasticity on the flow. Although the theory accounts for such subtle effects as the variation of the interphase drag due to excluded volume effects near the wall and the lubrication energy losses as particles collide with the wall, the primary results of the theory depend only on the granular transport mechanisms and the viscous dissipation of granular kinetic energy by the gas. This energy dissipation has been determined as a function of particle volume fraction and a Reynolds number based on the granular temperature by Verberg & Koch (2006) based on the detailed hydrodynamic flows produced by agitated solids.

Our theory deviates from our simulation results at small Stokes numbers and/or small values of the coefficient of restitution. It is of interest to consider the origins of these deviations so that a better theory might be proposed in the future. In the averaged equation for the gas phase we made the crude approximation that the viscous stress in the gas was given by a constitutive equation developed by Happel & Brenner (1965) for suspensions with vanishingly small Stokes numbers, cf. (2.27). We can extract from the simulations the viscous contributions to the stress, including the contributions of the particle stresslets, and thereby provide a direct test of this aspect of the theory. Figure 12 compares the viscous stress predicted by the Happel & Brenner theory with the results of LB simulations for $St = 30$; the viscous

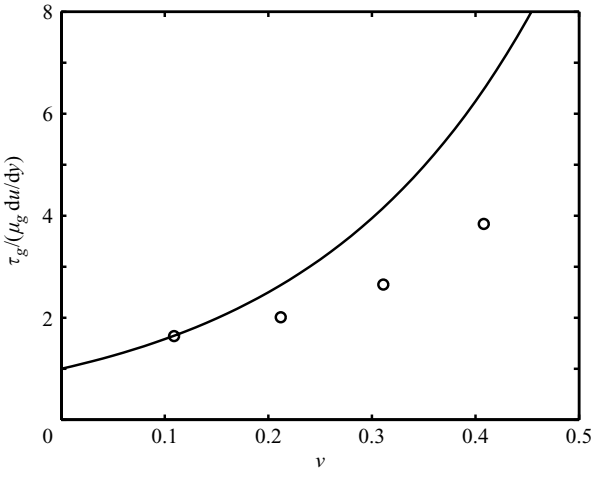

FIGURE 12. Comparison of the viscous contribution to the stress measured from ○, LB simulations and —, the Happel & Brenner (1965) prediction. The circles show the total viscous contribution to stress normalized by fluid viscosity μ_g and the shear rate $\mathrm{d}u/\mathrm{d}y$ obtained from LB simulations at $St = 30$. The line is the prediction of the ratio of the suspension viscosity at low Reynolds and Stokes numbers to the fluid viscosity.

stress was found to be insensitive to St for $St \gg 1$. The viscous stress obtained from simulations at high Stokes numbers has the same order of magnitude as that for $St \ll 1$ and has a qualitatively similar dependence on particle volume fraction. However, the high-Stokes-number viscous stress is systematically lower than the Happel & Brenner prediction. This is not surprising because particle inertia would be expected to inhibit the formation of particle clusters that contribute much of the viscous stress in low-Stokes-number suspensions at high volume fractions (Verberg & Koch 2006). It should be noted, however, that the viscous stresses have a negligible effect on the flow profiles presented in this paper. The viscous stress remains at least an order of magnitude smaller than the particle-phase stress even at $St = 10$ where the deviation of the simulation profiles from the theoretical predictions is substantial.

When the theory deviates from the simulations, the stress derived from the simulation is still dominated by the kinetic and collisional contributions from the particulate phase. The primary difference between the theory and simulation at small Stokes numbers ($St = 10$ in figure 2) or small coefficients of restitution ($St = 30$ and $e = 0.8$ in figure 11) is that the theory predicts a more pronounced collapse of the granular temperature and increase of the particle volume fraction in the centre of the channel. These deviations occur when $T^{1/2}/\Gamma a < 1$. The particle volume fraction profile is determined by the condition, derived from the cross-stream momentum balance, that the granular pressure should remain constant across the gap. If we use the local flow conditions predicted by the simulations to compute the kinetic and collisional contributions to the (y, y)-component of the stress, we find that the theoretical predictions for the kinetic stress are in very good agreement with the simulated stress even for $St = 30$ and $e = 0.8$ (corresponding to $e_{eff} = 0.69$). However, the theory underpredicts the collisional contribution to the stress significantly. These observations are consistent with studies of granular flows where it is found that kinetic theory breaks down at $e \approx 0.7$ and that the deviations from the theory involve collisional stresses and not kinetic stresses (Bizon *et al.* 1999). Bizon *et al.* noted that

the collisional stresses deviate from the kinetic theory because of two effects. (i) The spatial distribution of inelastic particles has more close pairs than predicted for elastic hard spheres. (ii) Pairs of inelastic particles have correlated velocities. The first effect tends to increase the collisional stress whereas the latter reduces it. Simulations of granular flows yield a collisional pressure that is larger than predicted by kinetic theory because the correlation in the velocity of neighbouring particles has the predominant effect (Bizon *et al.* 1999; Mitarai & Nakanishi 2007). In contrast, our simulations indicate that the collisional stress in a gas–solid suspension is underpredicted by the kinetic theory. We believe that the hydrodynamic forces associated with the mean gas flow and the fluctuating gas flows induced by particles may lead to greater relative velocities of neighbouring particles than are seen in granular flows without a gas. The increased spatial correlation of particles induced by lubrication forces and inelastic collisions would then be expected to increase the collisional stress relative to the predictions of a kinetic theory using hard-sphere pair distribution function. Thus, a theory that captures the spatial correlations of particles in a sheared gas–solid suspension and the resulting collisional stresses may be able to extend the current predictions to even lower Stokes numbers and coefficients of restitution.

R. V. and D. L. K. are grateful to Anthony J. C. Ladd for sharing his particle-suspension code (Susp3D) and for help in modifying it. R. V. and D. L. K. also acknowledge computational resources of the Cornell Theory Center, which receives funding from Cornell University, New York State, federal agencies, foundations, and corporate partners. They were supported by NASA grant NAG3-1853 and US Department of Energy grant DE-FG02-03-ER46073. H. X. and M. Y. L. were supported by NASA grants NAG3-2705 and NCC3-797.

Appendix. Boundary conditions for the solid phase at the bumpy boundary

Here, we derive expressions for the stress and the flux of fluctuation energy ('heat' flux) for a flow of inelastic smooth spheres in a viscous gas at a bumpy wall shown in figure 1, by considering the momentum and energy transfer during each collision between a flow sphere and a wall bump and integrating over all such collisions. For the problem to remain tractable, we neglect the effect of other nearby flow spheres and wall bumps on the hydrodynamic interaction between the colliding pair and treat them as in an infinite medium. We also neglect particle rotation and the tangential lubrication force as it is much smaller than the normal force. Even with the above simplifications, the problem is still complicated. The main difficulty is that the velocity distribution of the flow spheres just before colliding with the wall is unknown. In principle, we could solve the Boltzmann equation at the boundary to find this velocity distribution. The task is, however, formidable, especially when dealing with non-flat walls as in our case. Fortunately, the expressions for the stress and the heat flux at the wall, being integrals over the velocity distribution, are not sensitive to the exact functional form of the velocity distribution. For example, in Xu (2003), the differences between calculated stresses and heat fluxes at a flat frictional wall using three very different velocity distributions for the colliding spheres are surprisingly small. Therefore, it is a common practice to use a velocity distribution obtained from solving the Boltzmann equation in an infinite domain when calculating the boundary conditions for granular flows. The other difficulty encountered when deriving boundary conditions is the orders of truncation. As it is not usually possible to evaluate the integrals in closed form, especially when there is slip between the flowing particles and the solid walls,

some form of expansion and truncation of terms, e.g. in powers of the inelasticity $1-e$, the dimensionless slip $u_{slip}/T^{1/2}$ at the wall, and parameters characterizing the roughness of the wall (see details later in this Appendix), must be invoked. It is therefore necessary to keep the boundary conditions to the same order of the parameters used in truncation as the hydrodynamic equations themselves. We show below how these problems were handled when deriving the boundary conditions for our cases.

Sundararajakumar & Koch (1996) calculated the energy loss in a collision between two elastic spheres in a viscous gas. Their result shows that the energy loss can be written in the form of an equivalent coefficient of restitution

$$e_{vis} = 1 - \frac{A}{St_n}, \tag{A 1}$$

where $St_n \equiv \tau_v u_n/a$ is the Stokes number based on u_n, the relative velocity between two spheres along the line of centre before collision; $A = \log(\delta_0/\lambda) - 1.28$ is a constant; $\delta_0 = 0.1a$ is the distance threshold above which the hydrodynamic forces between the two spheres can be neglected, and λ is the mean free path of the gas molecules. The loss of kinetic energy during a collision is $(1-e_{vis}^2)u_n^2/2$. For inelastic spheres, it is straightforward to show that the loss of kinetic energy due to the combined effect of inelasticity and viscous damping is $(1-e_{eff}^2)u_n^2/2$ with the effective coefficient of restitution given by

$$e_{eff} = e e_{vis} = e(1 - A/St_n), \tag{A 2}$$

where e is the coefficient of restitution due to inelasticity. Note that e_{eff} depends on the collision velocity through e_{vis}.

As shown by Jenkins & Richman (1986), the collisional momentum transfer per unit area at a bumpy wall consisting of spheres can be calculated by integrating over all possible collisions

$$\boldsymbol{M} = \frac{4\chi}{\pi}\frac{\sigma^2}{(d+s)^2} m \int_{\boldsymbol{g}\cdot\boldsymbol{k}>0} (1+e_{eff})\boldsymbol{k}(\boldsymbol{g}\cdot\boldsymbol{k})^2 f(\boldsymbol{C},\, \boldsymbol{p}+\bar{\sigma}\boldsymbol{k})\,\mathrm{d}\boldsymbol{C}\,\mathrm{d}\boldsymbol{k}, \tag{A 3}$$

where σ is the diameter of flow spheres, d is the diameter of wall spheres, $\bar{\sigma} = (d+\sigma)/2$ is the distance between sphere centres at collision, s is the distance between the edges of wall spheres, m is the mass of the flow sphere, the factor χ accounts for the change of collision probability due to the finite size of the spheres and the shielding effect of other particles, $\boldsymbol{k}$ is the unit vector pointing from the centre of the wall sphere to the centre of the flow sphere, $\boldsymbol{g} = \boldsymbol{v} - \boldsymbol{C}$ is the velocity of the flow sphere relative to the wall sphere, $\boldsymbol{v}$ is the relative velocity between the mean flow and the wall, $\boldsymbol{C}$ is the fluctuation velocity of the colliding flow sphere relative to the mean flow, and $f(\boldsymbol{C},\, \boldsymbol{p}+\sigma\boldsymbol{k})$ is the velocity distribution of flow spheres at the position of collision. We adopt the modified Maxwellian velocity distribution function given by Richman (1988) for inelastic spheres

$$f(\boldsymbol{C},\, \boldsymbol{p}+\bar{\sigma}\boldsymbol{k}) = \frac{n}{(2\pi T)^{3/2}}\left\{1 + \frac{\bar{\sigma}}{T}[(\boldsymbol{k}\cdot\nabla - \boldsymbol{N}\cdot\nabla)\boldsymbol{u}]\cdot\boldsymbol{C} - \sqrt{\frac{2}{\pi}}\frac{\sigma B}{T^{3/2}}\boldsymbol{C}\cdot\hat{\boldsymbol{D}}\cdot\boldsymbol{C}\right\}\mathrm{e}^{-C^2/2T}, \tag{A 4}$$

in which n is the number density of flow spheres, T is the granular temperature at the boundary, $\boldsymbol{N}$ is the unit vector normal to the wall, $\boldsymbol{u}$ is the mean velocity of the flow

spheres, B is a known function of particle volume fraction, and $\hat{\boldsymbol{D}}$ is the deviatoric part of the symmetric velocity gradient of flow spheres.

Similarly, the energy loss per unit wall area can be written as

$$D = \frac{2\chi}{\pi}\frac{\sigma^2}{(d+s)^2} m \int_{\boldsymbol{g}\cdot\boldsymbol{k}>0} \left(1-e_{eff}^2\right)\left(\boldsymbol{g}\cdot\boldsymbol{k}\right)^3 f(\boldsymbol{C},\, \boldsymbol{p}+\bar{\sigma}\boldsymbol{k})\,\mathrm{d}\boldsymbol{C}\,\mathrm{d}\boldsymbol{k}. \tag{A 5}$$

The integrals (A 3) and (A 5) are evaluated by substituting (A 4) into them and noting that $St_n = 2\tau_v(\boldsymbol{g}\cdot\boldsymbol{k})/\sigma$ in the expression for e_{eff}. The detailed procedure is similar to the derivation of boundary conditions for the flow of smooth inelastic spheres over a wall with the same geometry in the absence of viscous gas, as shown in Xu (2003). We give only an outline here. We first note that for the hexagonal configuration of wall spheres, the penetration angle $\theta \equiv \sin^{-1}[(\mathrm{d}+s)/2\sigma]$ varies with the azimuthal angle about the normal vector N. Since the change of θ is rather small for this configuration, we approximate the integrals by first integrating over θ to obtain the average $\bar{\theta}$ and then carrying other integrations with this fixed $\bar{\theta}$. After integrating over $\mathrm{d}\boldsymbol{C}$, we encounter in the integrand, error functions and exponential functions that involve the dimensionless slip velocity $v\sin\bar{\theta}/\sqrt{T}$. The second approximation is to expand these functions as power series of $v\sin\bar{\theta}/\sqrt{T}$ and truncate at appropriate orders before integrating over $\mathrm{d}\boldsymbol{k}$. In flows with a mean gas pressure gradient or a streamwise body force, the slip velocity can be large, i.e. $v/\sqrt{T} \sim O(1)$. However, we notice that most practical bumpy boundaries satisfy $\sin\bar{\theta} \ll 1$. We therefore retain only terms that are of order $\sin^2\bar{\theta}$ and neglect higher-order terms in the integral. The final result of the shear and normal stresses are

$$S = \tfrac{1}{2}(1+e)\rho\chi T\frac{v}{\sqrt{T}}\sqrt{\frac{2}{\pi}}\frac{2}{3}\left(\frac{2}{1+\cos\bar{\theta}}-\cos\bar{\theta}\right)\left(1-\frac{1}{4}\sqrt{\frac{\pi}{2}}\frac{e}{1+e}\frac{A}{St_T}\right), \tag{A 6}$$

and

$$N = \tfrac{1}{2}(1+e)\rho\chi T\left(1+\tfrac{1}{4}\sin^2\bar{\theta}\,\frac{v^2}{T}\right)\left(1-\frac{1}{2\sqrt{2\pi}}\frac{e}{1+e}\frac{A}{St_T}\right), \tag{A 7}$$

where $\rho = nm$ is the density of the solid phase and $St_T \equiv \tau_v\sqrt{T}/\sigma$ is the Stokes number based on particle fluctuation velocity. The energy loss is

$$D = \tfrac{1}{2}\rho\chi T^{3/2}\frac{1}{1+\cos\bar{\theta}}\left[2\sqrt{\frac{2}{\pi}}(1-e^2)+e^2\frac{A}{St_T}\left(1-\sqrt{\frac{2}{\pi}}\frac{A}{4St_T}\right)\right]. \tag{A 8}$$

The unknown factor χ can be eliminated by using the ratio of shear to normal stress and the dimensionless energy flux Q at the boundary

$$\frac{Q}{N\sqrt{T}} = \frac{Sv-D}{N\sqrt{T}}. \tag{A 9}$$

The expressions are given as (2.32) and (2.33) in § 2.3.

REFERENCES

Acrivos, A. & Chang, E. 1986 A model for estimating transport quantities in two-phase materials. *Phys. Fluids* **29**, 3–4.

Anderson, T. B. & Jackson, R. 1967 A fluid mechanical description of fluidized beds. *Ind. Engng Chem. Fundamentals* **6**, 527–539.

Batchelor, G. K. 1970 The stress system in a suspension of force-free particles. *J. Fluid Mech.* **41**, 545–570.

Bizon, C., Shattuck, M. D., Swift, J. B. & Swinney, H. L. 1999 Transport coefficients for granular media from molecular dynamics simulations. *Phys. Rev.* E **60**, 4340–4351.

Bolio, E. J., Yasuna, J. A. & Sinclair, J. L. 1995 Dilute, turbulent gas–solid flow in risers with particle–particle interactions. *AIChE J.* **41**, 1375–1388.

Brinkman, H. C. 1949 A calculation of the viscous force exerted by a flowing fluid on a dense swarm of particles. *Appl. Sci. Res.* A **1**, 27–34.

Carman, P. C. 1937 The determination of the specific surface area of powder I. *J. Soc. Chem. Ind.* **57**, 225–236.

Carnahan, N. F. & Starling, K. E. 1969 Equation of state for nonattracting rigid spheres. *J. Chem. Phys.* **51**, 635–636.

Clift, R., Grace, J. R. & Weber, M. E. 1978 *Bubbles, Drops, and Particles*. Academic.

Dasgupta, S., Jackson, R. & Sundaresan, S. 1994 Turbulent gas–particle flow in vertical risers. *AIChE J.* **40**, 215–228.

Ergun, S. 1952 Pressure drop through granular beds. *Chem. Engng Prog.* **48**, 84–88.

Garzó, V. & Dufty, J. W. 1999 Dense fluid transport for inelastic hard spheres. *Phys. Rev.* E **59**, 5895–5911.

Goldhirsch, I., Noskowicz, S. H. & Bar-Lev, O. 2005 Nearly smooth granular gases. *Phys. Rev. Lett.* **95**, 068002.

Gopinath, A., Chen, S. B. & Koch, D. L. 1997 Lubrication flows between spherical particles colliding in a compressible non-continuum gas. *J. Fluid Mech.* **344**, 245–269.

Happel, J. & Brenner, H. 1965 *Low Reynolds Number Hydrodynamics*. Prentice-Hall.

Hill, R. J., Koch, D. L. & Ladd, A. J. C. 2001*a* The first effects of fluid inertia on flows in ordered and random arrays of spheres. *J. Fluid Mech.* **448**, 213–241.

Hill, R. J., Koch, D. L. & Ladd, A. J. C. 2001*b* Moderate-Reynolds-number flows in ordered and random arrays of spheres. *J. Fluid Mech.* **448**, 243–278.

Hopkins, M. A. & Louge, M. Y. 1991 Inelastic microstructure in rapid granular flows of smooth disks. *Phys. Fluids* A **3**, 47–57.

Jenkins, J. T. 2001 Boundary conditions for collisional grain flows at bumpy, frictional walls. In *Granular Gases* (ed. T. Pöschel & S. Luding), pp. 125–139. Springer.

Jenkins, J. T. & Richman, M. W. 1985 Grad's 13-moment system for a dense gas of inelastic spheres. *Arch. Rat. Mech. Anal.* **87**, 355–377.

Jenkins, J. T. & Richman, M. W. 1986 Boundary conditions for plane flows of smooth, nearly elastic, circular disks. *J. Fluid Mech.* **171**, 313–328.

Koch, D. L. & Sangani, A. S. 1999 Particle pressure and marginal stability limits for a homogeneous monodisperse gas fluidized bed: kinetic theory and numerical simulations. *J. Fluid Mech.* **400**, 229–263.

Kumaran, V. 2006 The constitutive relation for the granular flow of rough particles, and its application to the flow down an inclined plane. *J. Fluid Mech.* **561**, 1–42.

Liss, E. D., Conway, S. L. & Glasser, B. J. 2002 Density waves in gravity-driven granular flow through a channel. *Phys. Fluids* **14**, 3309–3326.

Louge, M. Y., Jenkins, J. T. & Hopkins, M. A. 1990 Computer simulations of rapid granular shear flows between parallel bumpy boundaries. *Phys. Fluids* A **2**, 1042–1044.

Louge, M. Y., Mastorakos, M. & Jenkins, J. T. 1991 The role of particle collisions in pneumatic transport. *J. Fluid Mech.* **231**, 345–359.

Louge, M. Y., Jenkins, J. T. & Hopkins, M. A. 1993 The relaxation of the second moments in rapid shear flows of smooth disks. *Mech. Mat.* **16**, 199–203.

Louge, M. Y., Jenkins, J. T., Reeves, A. & Keast, S. 2000 Microgravity segregation in collisional granular shearing flows. In *Proc. IUTAM Symp. on Segregation in Granular Materials* (ed. A. D. Rosato & D. L. Blackmore), pp. 103–112. Kluver.

Louge, M. Y., Jenkins, J. T., Xu, H. & Arnarson, B. Ö. 2001 Granular segregation in collisional shearing flows. In *Mechanics for a New Millennium* (ed. H. Aref & J. Phillips), pp. 239–252. Kluver.

Lun, C. K. K., Savage, S. B., Jeffrey, D. J. & Chepurniy, N. 1984 Kinetic theories for granular flow: inelastic particles in Couette flow and slightly inelastic particles in a general flow field. *J. Fluid Mech.* **140**, 223–256.

Maxwell, J. C. 1879 On stresses in rarified gases arising from inequalities of temperature. *Phil. Trans. R. Soc. Lond.* **170**, 231–256.

Mitarai, N. & Nakanishi, H. 2007 Velocity correlations in dense granular shear flows: effects of energy dissipation and normal stress. *Phys. Rev.* E **75**, 031305.

Mueth, D. M., Debregeas, G. F., Karczmar, G. S., Eng, P. J., Nagel, S. R. & Jaeger, H. 2000 Signatures of granular microstructure in dense shear flows. *Nature* **406**, 385–389.

Onoda, G. Y. & Liniger, E. G. 1990 Random loose packing of uniform spheres and the dilatancy onset. *Phys. Rev. Lett.* **64**, 2727–2730.

Richman, M. W. 1988 Boundary conditions based upon a modified Maxwellian velocity distribution function for flows of identical, smooth, nearly elastic spheres. *Acta Mech.* **75**, 227–240.

Richman, M. W. & Chou, C. S. 1988 Boundary effects on granular flows of smooth disks. *Z. Angew. Mech. Phys.* **39**, 885–901.

Sangani, A. S. & Behl, S. 1989 The planar singular solutions of Stokes and Laplace equations and their application to transport processes near porous surfaces. *Phys. Fluids* A **1**, 21–37.

Sangani, A. S., Mo, G., Tsao, H.-K. & Koch, D. L. 1996 Simple shear flows of dense gas–solid suspensions at finite Stokes numbers. *J. Fluid Mech.* **313**, 309–341.

Sela, N. & Goldhirsch, I. 1998 Hydrodynamic equations for rapid flows of smooth inelastic spheres, to Burnett order. *J. Fluid Mech.* **361**, 41–74.

Sinclair, J. L. & Jackson, R. 1989 Gas–particle flow in a vertical pipe with particle–particle interactions. *AIChE J.* **39**, 1473–1486.

Smart, J. R. & Leighton Jr., D. T. 1989 Measurement of the hydrodynamic surface roughness of noncolloidal spheres. *Phys. Fluids* A **1**, 52–60.

Sundaram, S. & Collins, L. R. 1997 Collision statistics in an isotropic particle-laden turbulent suspension. I. Direct numerical simulations. *J. Fluid Mech.* **335**, 75–109.

Sundararajakumar, R. R. & Koch, D. L. 1996 Non-continuum lubrication flows between particles colliding in a gas. *J. Fluid Mech.* **313**, 283–308.

Torquato, S. 1995 Nearest-neighbor statistics for packings of hard spheres and disks. *Phys. Rev.* E **51**, 3170–3182.

Verberg, R. & Koch, D. L. 2006 Rheology of particle suspensions with low to moderate fluid inertia at finite particle inertia. *Phys. Fluids* **18**, 083303.

Wylie, J. J., Koch, D. L. & Ladd, A. J. C. 2003 Rheology of suspensions with high particle inertia and moderate fluid inertia. *J. Fluid Mech.* **480**, 95–118.

Xu, H. 2003 Collisional granular flows with and without gas interactions in microgravity. PhD dissertation, Cornell University.

Xu, H., Louge, M. & Reeves, A. 2003 Solution of the kinetic theory for bounded collisional granular flows. *Continuum Mech. Thermodyn.* **15** (4), 321–349.

Zarraga, I. S., Hill, D. A. & Leighton Jr, D. T. 2000 The characterization of the total stress of concentrated suspensions of noncolloidal spheres in Newtonian fluids. *J. Rheol.* **44**, 185–220.